Effect of thermal conductivity and viscosity of alumina and graphene-based nanofluids for advanced thermal studies

G. D. Gosavi [a,*], P. Sivamurugan [b], M. I. Shajahan [b], J. S. S. Allwin Ebinesar [c]
[a]*Research Scholar,Department of Mechanical Engineering, Vel Tech Rangarajan Dr. Sagunthala R&D Institute of Science and Technology, Chennai, 600062, India.*
[b]*Department of Mechanical Engineering, Vel Tech Rangarajan Dr. Sagunthala R&D Institute of Science and Technology, Chennai, 600062, India.*
[c]*Department of Biotechnology, Acharya Institute of Technology, Bangalore, Karnataka,560107, India*

The current study investigates the full development of nanofluids at different volume fractions (0.1 and 0.5 vol.), employing a two-step method, as potential advanced heat transfer fluids (HTF), with pure water (base fluid) and alumina and graphene nano flasks (GPN) as nanoparticles and cetyltrimethylammonium bromide (CTAB) as surfactant. The physicochemical properties of the nanofluid combinations were assessed via X-ray diffraction (XRD) analysis and scanning electron microscopy (SEM). Zeta potential analysis revealed an increase of up to +37 mV at 0.1 vol % for alumina/water CTAB nanofluid and +35 mV at 0.5 vol % of Graphene/water CTAB nanofluids. The results demonstrated that alumina and GPN nanofluids exhibited improved thermal conductivity and viscosity. The CTAB GPN/water nanofluid displayed maximum thermal conductivity enhancements of 27.48% and 33.79%, while the CTAB alumina/water nanofluid showed enhancements of 10.6% and 19.81% for 0.1 and 0.5 vol%, respectively. The maximum increment in viscosity were found to be 121.28% and 165.84% for the CTAB GPN/water nanofluid and 110.64% and 111.3% for the CTAB Alumina/water nanofluids at 70 °C, respectively. Consequently, this nanofluid can be regarded as a viable alternative to conventional fluids in high-temperature applications.

(Received March 13, 2025; Accepted July 4, 2025)

Keywords: Nanofluids, Graphene, Alumina, Thermal Conductivity, Viscosity

1. Introduction

Renewability and sustainability of energy technologies play a critical role in addressing increasing energy demands, and facilitating a greener, more sustainable future. Over the last few decades, many scientists have investigated different techniques to improve the systems performance of heat transfer. One strategy has been to tinker with various fin configurations and shall optimize their designs to improve the efficiency of these devices. Moreover, it has been determined that the selection of heat transfer working fluid in the system plays a key role in how fast heat transfer occurs. Energy exchange systems rely on heat transfer fluids whose physical properties such as thermal conductivity, viscosity, density, and heat capacity determine their effectiveness. The main disadvantage of heat-transfer fluids, which is complementary to experimental studies, is their low thermal conductivity. This property limits the full advantage for the efficient utilisation of such fluids in any energy-exchanging process [1-3].

The field of nanofluids has seen rapid growth in recent years, emerging as a promising area within nanotechnology that focuses on heat-transfer fluids. Researchers are delving into the fundamental principles that influence the thermophysical properties of these materials, particularly thermal conductivity and viscosity. The advancement of nanofluid technology has shown

* Corresponding author: gdgicoer@gmail.com
https://doi.org/10.15251/DJNB.2025.203.719

considerable potential for heat transfer applications, resulting in extensive research efforts in both academia and industry [4].

Nanofluid is a new type of liquid created by dispersing different kinds of nanoparticles in a base fluid. These nanoparticles can consist of metal oxides (like aluminum oxide and copper oxide), metals (such as silver and copper), carbon-based materials (including carbon nanotubes and graphene), and non-metallic substances (for example, boron nitride) [5]. The presence of dispersed nanoparticles significantly improves the thermal conductivity of the fluid, thanks to their excellent heat-conducting properties. Research on heat transfer with various nanofluid samples has indicated that their performance often surpasses theoretical predictions [6]. Scientists have employed a range of physical and chemical techniques to synthesize these nanoparticles [7], which are then analyzed using methods such as X-ray Diffraction (XRD), Scanning Electron Microscopy (SEM), and energy dispersive X-ray spectroscopy (EDAX). These techniques help confirm the nanoparticles' crystal structure, surface characteristics, size, and elemental composition [8].

In recent years, there has been a growing interest in the study of nanofluids, driven by the increasing demand for sustainable cooling solutions. To improve the properties of nanofluids, it is essential to create a formulation that is both stable and durable. When particles gather and form clusters, the risk of settling rises, which can lead to reduced suspension stability and a decline in important properties like thermal conductivity, viscosity, and heat capacity. The process of producing nanofluids involves several key stages, with preparation techniques that include magnetic stirring, ultrasonication, and frequency adjustments [9].

Nanofluids can be created using either a one-step or two-step process. The one-step method involves generating and dispersing nanoparticles simultaneously within a base fluid [11]. This technique often utilizes methods like chemical reduction, physical vapor deposition, or laser ablation directly in the liquid medium. By integrating the synthesis and dispersion of nanoparticles into a single phase, this method reduces the likelihood of particle agglomeration. Consequently, the one-step technique produces nanofluids that exhibit better stability and a more uniform distribution of particles throughout the fluid [12]. This approach also removes the need for separate stages of nanoparticle production and dispersion, resulting in an overall improvement in nanofluid quality.

The two-step method enhances stability and ensures an even distribution of nanoparticles in the liquid. The resulting nano powders, measured by volume or weight concentration, are blended into a base liquid like water or glycols. The process starts with magnetic stirring, which is then followed by ultrasonication or homogenization. In certain instances, a surfactant is added to improve the stability of the nanofluid. This approach is especially effective for large-scale production [13].

The strong gravitational and van der Waals forces that promote particle aggregation remain a significant practical challenge when aiming to create a stable suspension. For high-quality suspensions, fine particles generally need to possess two key characteristics: the principle of penetration and zeta potential. Research indicates that there are three commonly accepted methods for achieving stable suspensions [10], which are as adding surfactants, pH control and ultrasonic vibration.

Surfactants are commonly used to enhance nanofluid stability by preventing nanoparticle aggregation through electrostatic or steric repulsion. However, excess surfactants increase viscosity and reduce thermal conductivity, while insufficient amounts cause agglomeration. Balancing surfactant levels is essential for stability and maintaining nanofluid properties [14]. The study examined water-dispersed alumina nanoparticles (0.1 wt. %) with CTAB and SDBS, finding that SDBS at its critical micelle concentration (0.064 wt. %) provided optimal stability. This concentration ensures effective dispersion and high stability across different pH levels [15].

Surfactant concentration and pH levels vary with the specific nanoparticles and base fluid used [16]. Nanofluids have different optimal pH levels influenced by the nanoparticles' surface charge, size, and composition. Managing pH is crucial for maintaining suspension stability, minimizing aggregation, and optimizing nanofluid properties. Various studies have examined the impact of sonication duration on nanofluid stability [17]. Maximizing the absolute value of zeta potential enhances repulsive forces between particles, with values of −30 mV or +30 mV considered standards for maintaining dispersion over time [18]. Said [19] found that changing sonication time from 20 to 200 min did not consistently improve nanofluid stability. AlZnO nanofluid with

surfactant showed higher zeta potential than without, indicating better dispersion stability, reduced agglomeration, and controlled nanoparticle size.

Compared to other magnetic methods and stirrers, the ultrasonic bath, processor, and homogenizer are powerful tools for breaking particle aggregation. The fabrication of CuO-water nanofluids has been explained by Priya et al. [20] utilizing ultrasonication and Tiron as a surfactant. Measurements of the colloids' zeta potentials confirmed their stability; these readings were 30 mV, which is more than enough to guarantee colloidal stability.

Various studies are conducted with different nanofluids mixed with water. A Study was conducted with alumina nanofluids. The results indicate that the thermal conductivity of an Alumina/water nanofluid increases with temperature and volume fraction while decreasing with sphericity. A sensitivity analysis reveals that temperature, sphericity, and volume fraction are the variables most susceptible to modification. Temperature variations of merely 1% can occasionally induce a change in thermal conductivity of up to 4%. The utilization of spherical particles facilitates greater stability in the thermal conductivity of the nanofluid, and the sensitive volume fraction range that can cause significant fluctuations in thermal conductivity lies between 2.5% and 5.5% [21].

Another study was conducted with Al_2O_3 nanoparticles based nanofluid. The Wiedemann-Franz law was used to link electrical conductivity to thermal conductivity. Findings showed that the nanofluid with 1% SDBS was the most stable, while settling occurred in the fluid containing 0.75 vol.% of Al_2O_3 nanoparticles, which exhibited higher viscosity. Rheological tests indicated that nanofluid viscosity initially decreased as shear rate increased, demonstrating shear thinning behavior. The addition of nanoparticles to the base liquid enhanced electrical conductivity up to 0.2 vol. % of Al_2O_3 nanoparticles, after which it declined [22].

Nanoparticles of α-Al_2O_3, which have excellent thermal conductivity, were created as part of the research using the sol-gel method. Analyzing the materials' X-ray diffraction spectra validated their crystal structure and alpha (α) phase. According to the calculations, the average size of the crystals was 55.5 nm. Despite their non-standard form, the nanoparticles were found to be 40 to 60 nm in size by transmission electron microscopy. Within the temperature range of 30 ◦C to 1200 °C, thermogravimetric study revealed a weight loss of less than 0.5% [23].

Nanofluids derived from graphene are considered highly promising due to the exceptional inherent properties of these nanomaterials. When evaluating the potential of graphene-based nanofluids as effective and reliable heat transfer media, it is crucial to consider not only their thermal characteristics but also their viscosity and overall rheological behavior, which are key components of their thermophysical profile [24].

Increasing graphene oxide concentration from 0.01 to 0.1 wt. % linearly raises both particle size and viscosity of nanofluids. A study was conducted by Esfahani, et al. [25] where substantial increase in particle size and viscosity occurs at 0.5 wt. %. Thermal conductivity, measured at various temperatures, is affected by particle size distribution and viscosity. All graphene oxide nanofluids exhibited higher thermal conductivity than water. Enhancements of 8.7% and 18.9% were observed at 25 °C with concentrations of 0.01 wt. % and 0.1 wt. %, respectively. A concentration of 0.5 wt. % resulted in a 19.9% increase. These findings indicate an optimal graphene oxide concentration for maximizing thermal conductivity, beyond which no significant improvement is observed.

Another study was conducted with Graphene nanoplatelet (GNP) nanofluids with 25°C, and 0.056% volume percentage of deionized water increased thermal conductivity by 14% and when heated to 50 °C, conductivity improved 64%. Also, GNP nanofluids have 4.2% to 14.2% higher thermal conductivity than water. Viscosity decreases with temperature and increases with nanoparticle mass fraction, shear-thinning according to the Power Law model of viscosity with a flow behaviour index of 0.9 [26].

Table 1. Summary of various Studies with graphene based nanofluids.

Ref	Base fluid	Surfactants	Summary
[27].	Deionized Water	Triton X-100	With 0.06 weight%, nano fluid is 6 months stable and maximal enhancement is roughly 36.78%.
[28].	Deionized Water	SDBS, SDS, GA, CTAB	60 min sonication gives high stability with 0.1% GNP addition.
[29].	Deionized Water	SDS	The surface tension of saline solution decreases maximum by 21.5% when GNP at 25°C is added.
[30].	Distilled Water	SDS	For concentrations up to 0.02 wt%, addition of graphene and the SDS did not significantly modify the thermal conductivity of the nanofluids or increase viscosity.
[31].	Water	Sodium deoxycholate	For 0.5 vol%, the highest increase of thermal conductivity is 29%.
[32].	Water	CTAB, SDBS, and GA	After 60 days storage, the stability of nanofluid with GA surfactants exhibited better results than those based on SDBS, CTAB, and absence of surfactants.
[33].	Deionized Water	GA	Using 0.2% graphene/water nanofluids allowed a maximum increase in the heat transfer coefficient of 29%.
[34].	Water	SDBS	The results showed that the functionalization method has a significant impact on the thermal conductivity.
[35].	Kerosene	-	At 20 °C, the thermal conductivity was 0.111 W/(mK), but at 60 °C, it increased to 0.162 W/(mK).

Consequently, there has been limited exploration of utilizing Graphene and Al_2O_3 nanofluid, highlighting a research gap in past experimental studies, particularly this investigation comparing the metal oxide (alumina) and carbon group (Graphene), where carbon group performs well than metal oxide. In the current research, stabilization performance of Graphene and Al_2O_3 containing water-based nanofluids have been investigated. In comparison with previous works, the current method is significantly easy and does not need any advanced facilities. Nanofluids are prepared using two step technique and samples are tested for the property enhancement. Therefore, the present study systematically characterized and tested the material with an eye towards its thermo-physical characteristics and heat transfer effectiveness.

2. Materials and methods

2.1. Functionalization

Sigma-Aldrich supplied the commercially available aluminum oxide, graphene nanoflakes, CTAB, and deionized water used in this study are listed in the Table 1.

Table 1. Thermophysical properties of DI and nanomaterials.

Property	DI	Aluminum oxide	Graphene
Density, kg/m^3	997	3960	2600
Specific heat, J/kg K	4220	729	710
Thermal conductivity, W/mK	0.606	765	5300

Figs.1 (a) and (b) display the XRD patterns of the graphene and aluminum oxide nanoflakes, respectively. Additionally, Tables 2 and 3 provide detailed information on structural parameters such as full width at half maximum (FWHM), particle diameter, interatomic distance, surface area, specific surface area, and morphology index of aluminum oxide and graphene nanoflakes. Fig. 1a reveals that graphene exhibits a sharp, narrow peak at 2θ=25.62, corresponding to the (0 0 2) diffraction indices.

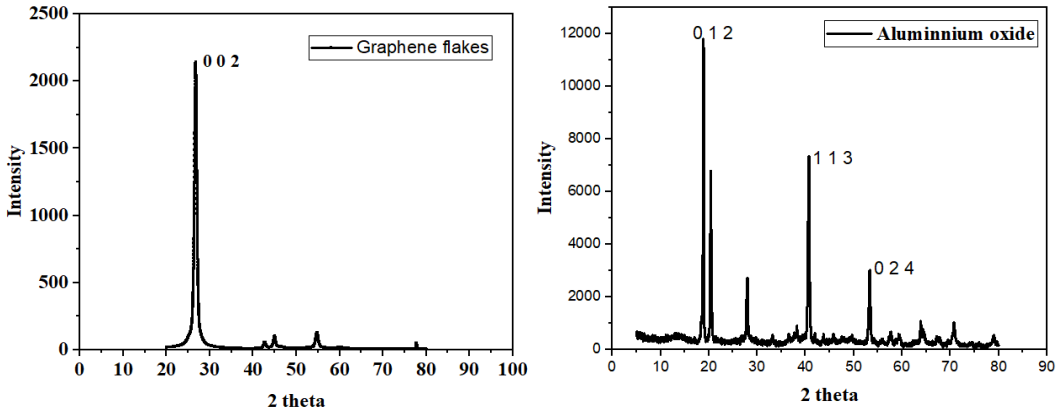

Fig. 1. (a and b). XRD Spectrogram for graphene nanoflakes and aluminium oxide nanoparticles.

In contrast, Fig. 1b shows peaks at 2θ values of 19.28, 20.21, 29.58, 40, 54, 66, and 74, indicating that the aluminum nanoflakes possess a polycrystalline, rhombohedral structure. The observed FWHM and morphology index values confirm that both the acquired graphene and aluminum nanoflakes are large and macrocrystalline in nature [36,37].

Table 2. XRD Details of aluminum oxide.

2θ	θ	cosθ	sinθ	FWHM (β) deg	FWHM (β) rad	βcosθ	size, D (nm)	d spacing, d (Å)	avg size (nm)	Sa (nm^2)	Vol (nm^3) X10^6	ssa (m^2/g)	sa/vol	Morphology index
26.52	13.26	0.97	0.22	0.1	0.001	0.001	81.62	3.35	65.03	53123.0	1.15	10.90	0.046	0.75
55	27.5	0.88	0.46	0.2	0.003	0.003	44.78	1.66	60.88	46562.8	9.45	11.64	0.049	0.60

Table 3. XRD Details of graphene nanoflakes.

2θ	θ	cosθ	sinθ	FWHM (β) deg	FWHM (β) rad	βcosθ	size, D (nm)	d spacing, d (Å)	Avg size (nm)	Sa (nm^2)	Vol (nm^3) x10^6	ssa (m^2/g)	sa/vol	Morphology index
19.28	9.64	0.98	0.16	0.1	0.001	0.0017	80.5	4.6	63.9	51351.9	1.09	11.09	0.04	0.753
20.21	10.15	0.94	0.17	0.2	0.003	0.0034	40.3	4.39	59.7	44884.6	8.94	11.86	0.05	0.604
29.58	14.79	0.96	0.25	0.15	0.002	0.0025	54.78	3.01	66.2	55136.3	1.21	10.70	0.04	0.670
40	20	0.93	0.34	0.1	0.001	0.0016	84.54	2.25	71.9	65098.5	1.56	9.85	0.04	0.753
54	27	0.89	0.45	0.15	0.002	0.0023	59.4	1.69	59.4	44376.3	8.79	11.93	0.05	0.670

The surface characteristics and elemental makeup of the chosen graphene nanoflakes and aluminum oxide specimens are displayed in Fig. 1.s 2 (a) and (b) and Fig. 1.s 3 (a) and (b), respectively. Analysis of the topography showed that the synthesized nanomaterials had irregular

forms with non-uniform surfaces. The samples' morphology was examined using SEM imaging. As shown in Fig.s 2a and 3a, the nanoflakes demonstrated a consistent, flake-like appearance without any noticeable damage or depressions. Additionally, this image suggests that the graphene nanoflakes were free from impurities.

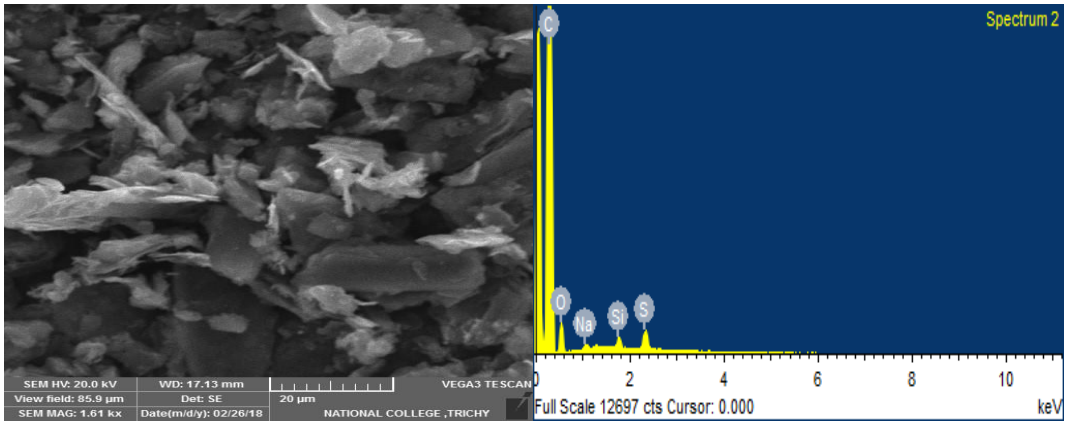

(a) *(b)*

Fig. 2. (a and b). SEM and EDAX spectrogram micrograph for graphene nanoflakes.

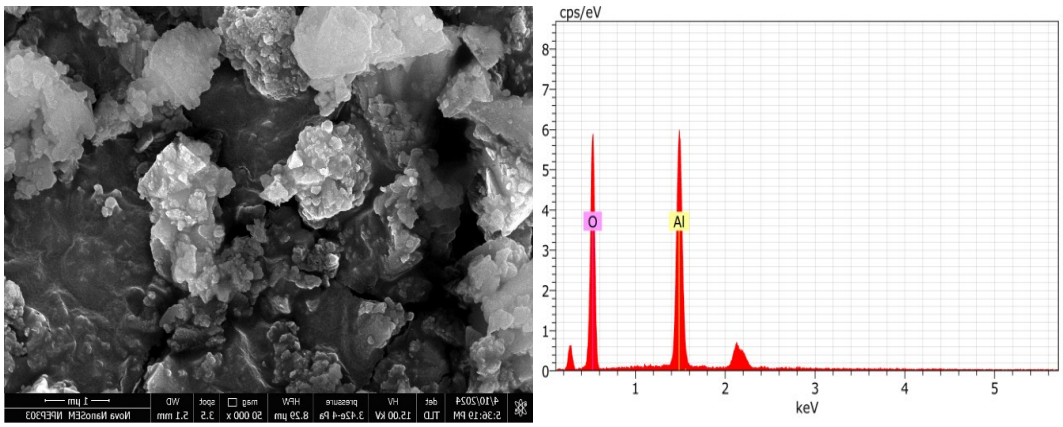

(a) *(b)*

Fig. 3. (a and b). SEM and EDAX spectrogram micrograph for aluminum oxide

The EDAX analysis results, depicted in Fig. 2b, showcase the elemental makeup of the graphene nanoflake sample. The results showed a high carbon (C) content of 90.07%, along with an oxygen (O) level of 9.43%, which was linked to oxidation that occurred during production. A trace amount of S (0.24%) was observed, while silicon and sodium were found to be negligible. The analysis confirmed the absence of other metallic or nonmetallic contaminants. Energy dispersive spectroscopy (EDAX) verified that the graphene nanoflakes were primarily composed of carbon, whereas the aluminum oxide was exclusively made up of aluminum and oxygen. This high level of purity is evidenced in Fig. 2b and Fig. 3b.

2.2. Preparation of nanofluid

The preparation of Al_2O_3/Water and GPN/Water nanofluids involves a two-step method. To begin, Al_2O_3 and GPN nanoparticles were measured and added to purified water at specific solid volume fractions (0.1% and 0.5%). Determining the necessary mass quantities was crucial before producing various nanofluid fractions [38]. A high-precision digital scale (Shimadzu Corporation, Japan) was employed to weigh the materials. Mass quantities were initially calculated using the nanoparticles' density. After introducing nanoparticles to water, the mixture underwent magnetic stirring (HS-12, HU) for about 1 hour. The suspensions were then processed using an ultrasonic processor (PS 30A 6 L, Germany) for approximately 3-4 hours. This step aims to break up particle

clusters, prevent settling, and ensure uniform particle distribution and suspension stability. Fig. 4 depicts the preparation process for the Al_2O_3/Water and GPN/Water nanofluids. All nanofluids were prepared in triplicate to ensure consistency. Cationic cetyltrimethylammonium bromide (CTAB) served as the surfactant at two different concentrations (0.1 vol. % and 0.5 vol.%). The amount of surfactant used in nanofluid preparation was 0.036 g of CTAB.

3. Determination of thermophysical properties

3.1. Thermal conductivity

The KD2-Pro thermal property analyzer (Decagon Devices Inc., USA) was utilised to assess thermal conductivity. This apparatus employs the transient hot wire method, a dynamic methodology that quantifies temperature elevations in a linear hot wire integrated within the test medium. The analyzer consists of a probe (1.3mm in diameter and 60mm in length), a thermoresistor, and a microprocessor for measuring probe conductivity. The instrument's sensor needle was calibrated before use, achieving an accuracy of ±5% by measuring the thermal conductivity of deionized water at 30°C, resulting in a value of 0.6 W/mK.

3.2. Viscosity

The Anton Paar MCR 102 is a modular compact rheometer for precise rheological measurements, including viscosity determination at controlled temperatures. With an electronically commutated (EC) motor, it offers exceptional low-torque sensitivity for delicate samples. Integrated temperature control options enable precise sample temperature management from -40°C to +200°C. This rheometer uses a cone-plate setup, ensuring versatility for different sample types. It features Tool master, which automatically recognizes installed geometries and transfers settings to the software, and T-Ready, which ensures thermal equilibrium before measurements. These features simplify operations and improve reproducibility. Using the right software for data analysis, the MCR 102 effectively measures viscosity changes over specific temperature ranges. Viscosity readings were recorded for Alumina/water and GPN/water, both with and without surfactant nanofluid, at intervals of 30°C, 40°C, 50°C, 60°C, and 70°C, respectively [40].

4. Stability analysis

Concentration significantly influences particle size in alumina-based water nanofluids, primarily due to aggregation and interactions between particles. At lower concentrations, such as 0.1%, the particles tend to stay more dispersed, which results in smaller effective sizes. However, when the concentration rises to 0.5%, particle aggregation becomes more noticeable because of increased collisions and van der Waals forces, leading to larger effective particle sizes [41]. To mitigate this issue, stabilization techniques like the use of surfactants such as CTAB can be employed. CTAB enhances thermal efficiency by improving heat transfer, and the overall performance of the nanofluid relies on finding the right balance between concentration and dispersion effectiveness.

4.1. Alumina based nanofluid

4.1.1. Particle size

Alumina/water nanofluids with 0.1% and 0.5% particle concentrations exhibited distinct behaviors when combined with the surfactant CTAB, which enhanced nanoparticle dispersion, minimized agglomeration, and promoted a uniform particle size. The 0.1% nanofluid demonstrated superior stability owing to reduced particle interaction, while the 0.5% nanofluid enhanced the viscosity and thermal conductivity. Thus, both the concentration and stabilization methods influenced the particle size distribution in these nanofluids, as shown in Fig. 5. The average diameter was 580 mm for alumina/water nanofluids with a 0.1% increase up to 880 mm for alumina/water nanofluids with a 0.5% CTAB inclusion.

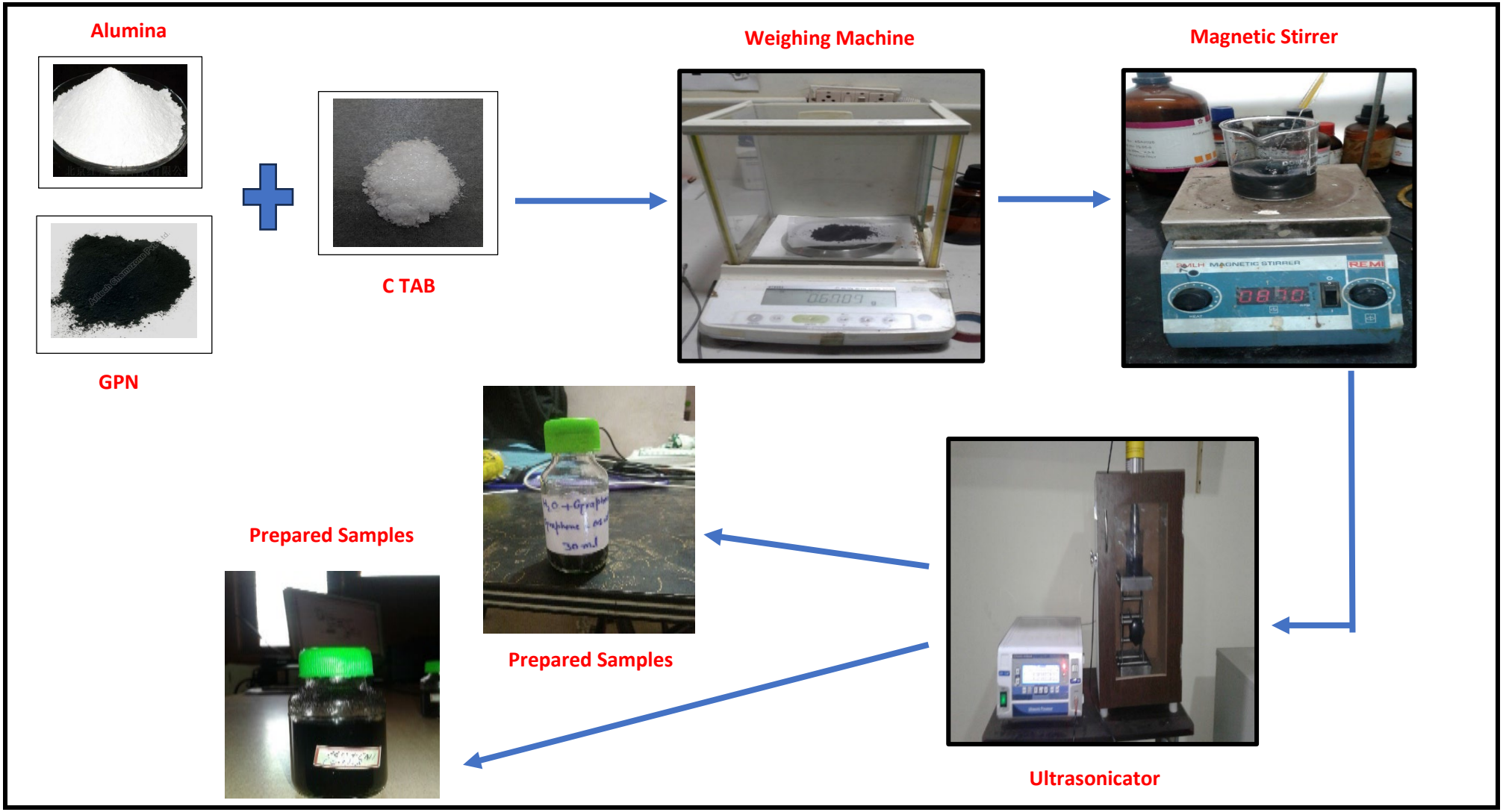

Fig. 4. Preparation steps for nanofluids.

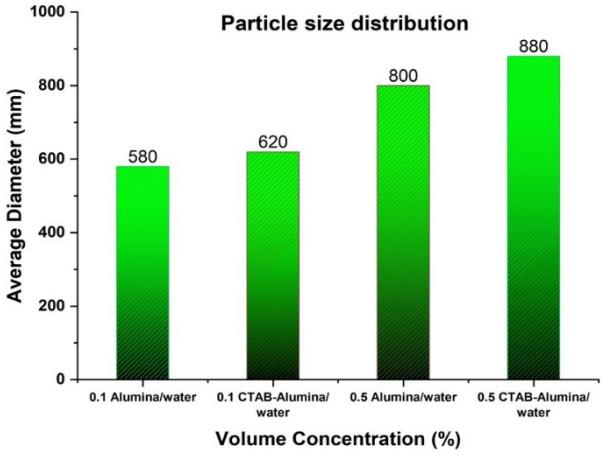

Fig. 5. Particle size distribution for alumina/ water nanofluids.

4.1.2. Zeta potential

The surface charge disparity between the unmodified and CTAB-modified Alumina/water nanofluid was investigated through zeta potential measurements at different volume percentages, with the pH held constant, as indicated in Fig. 6. The analysis revealed that the unmodified alumina/water nanofluid exhibited zeta potentials of approximately +31 and +28 mV at 0.1 and 0.5 vol %, respectively. Conversely, the CTAB-modified Alumina/water nanofluid displayed elevated zeta potentials, up to +37 mV at 0.1 vol % and +35 mV at 0.5 vol %. This increase in the positive charge of the CTAB-modified Al_2O_3/water nanofluid can be attributed to the exposure of the polar N+ ion end from CTAB, whereas the non-polar end facilitated the attachment of CTAB to alumina oxide nanoparticles through hydrogen bonding. It was also observed that the zeta potential values decreased as the volume percentage increased [42].

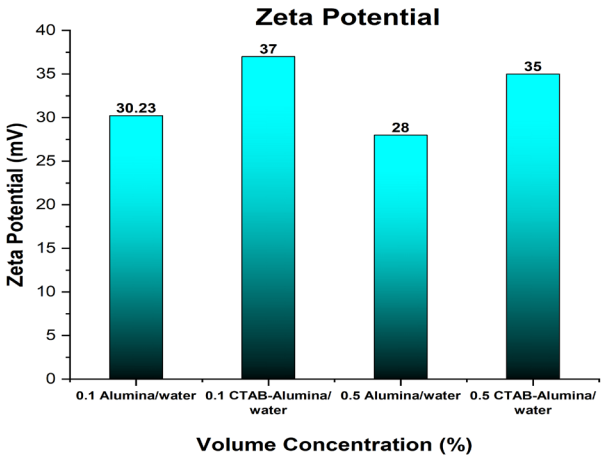

Fig. 6. Zeta potential for alumina/ water nanofluids.

4.1.3. pH value

The pH of alumina/water nanofluid becomes more acidic as its concentration increases from 0.1 vol % to 0.5 vol % due to the release of OH ions and attachment of H atoms from water molecules. The pH of alumina/water nanofluids varies with concentration due to nanoparticle interactions with the base fluid. At 0.1 vol % concentration, the pH remains close to water's natural pH (6.4) but at 0.5% (5.6), it deviates due to more nanoparticles. Adding CTAB, a cationic surfactant, stabilizes the nanofluid by reducing agglomeration, altering surface charge, and

potentially increasing pH due to its basic nature. CTAB also improves nanoparticle dispersion, enhancing thermal and rheological performance, and combining it with higher concentrations can optimize nanofluid properties for thermal applications as shown in Fig. 7 [43].

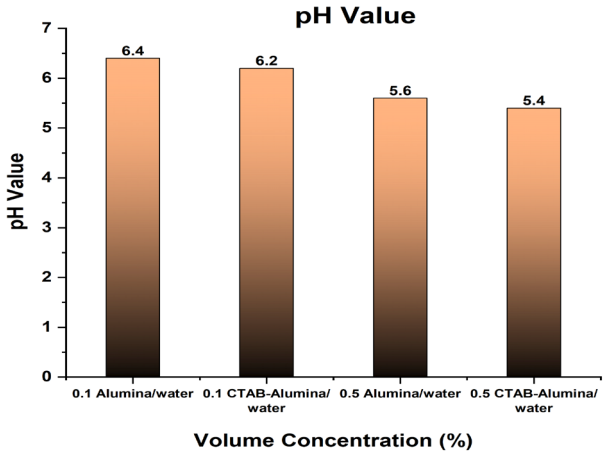

Fig. 7. pH Value for alumina/ water nanofluids.

4.2. Graphene based nanofluid

4.2.1. Particle size

In graphene/water nanofluids, the 0.1 vol% mixture typically demonstrates smaller particles due to its reduced graphene content, facilitating a more homogeneous nanofluid dispersion. Conversely, the 0.5 vol% solution tends to exhibit slightly larger particles, attributed to the increased graphene concentration, which may result in particle agglomeration. The incorporation of CTAB as a surfactant in these nanofluids generally enhances dispersion stability by mitigating particle aggregation. This process frequently leads to a reduction in graphene sheet dimensions. As a consequence, CTAB-containing solutions often produce smaller individual graphene particles compared to their surfactant-free counterparts.

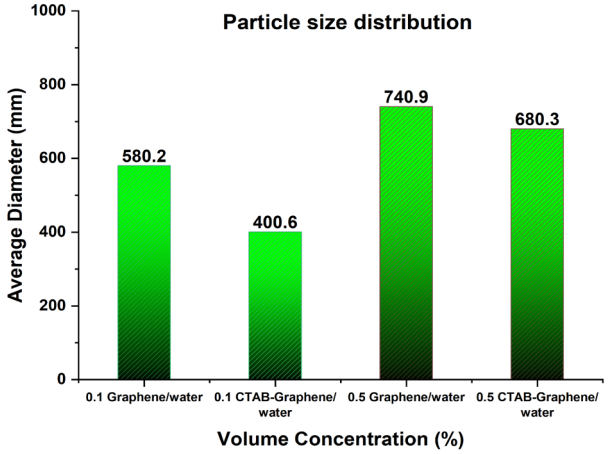

Fig. 8. Particle size distribution for GPN/ water nanofluids.

However, it is important to note that factors such as graphene concentration and dispersion quality continue to influence overall particle sizes (refer to Fig. 8). For instance, the average diameter of GPN/water nanofluids with 0.1% decreased from 580 mm to 400 mm upon the addition of 0.1%

CTAB. A similar trend was observed in GPN/water nanofluids with 0.5%, where the average diameter reduced from 740 mm to 680 mm following the inclusion of 0.5% CTAB.

4.2.2. Zeta potential

The graphene concentration influenced the zeta potential of graphene/water nanofluids. At 0.1 vol%, the potential ranged between -30 and -40 mV, suggesting moderate stability and adequate repulsive forces to inhibit nanoparticle aggregation. The potential increased to -40 to -60 mV at 0.5 vol%, improving suspension stability through enhanced electrostatic repulsion. These measurements indicate stable dispersion, crucial for maximizing nanofluid efficiency in heat transfer and energy applications. CTAB enabled the dispersion of pristine graphene in water by attaching its cationic quaternary ammonium head (N+) to graphene, creating a positive charge. This charge generates electrostatic repulsion between particles, preventing aggregation and boosting stability. The hydrophobic tail of CTAB also contributes to steric hindrance, further supporting dispersion. In pristine graphene, which lacks oxygen-containing functional groups, CTAB is stabilized through hydrophobic and van der Waals interactions. The resulting high positive zeta potential ensures excellent colloidal stability and dispersion, as illustrated in Fig. 9.

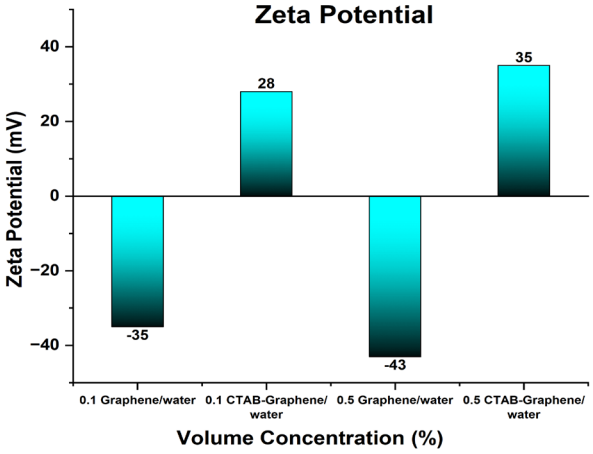

Fig. 9 Zeta potential for GPN/ water nanofluids.

4.2.3. pH value

For concentrations of 0.1 and 0.5 vol%, the pH usually stays near neutral (6-8). At 0.1 vol % concentration, the pH remains close to water's natural pH (6.5) but at 0.5% (6.1), it deviates due to more nanoparticles. Generally, the pH remains stable unless graphene particles undergo further functionalization. CTAB raises the solution's pH to alkaline levels. This happens when CTAB's positively charged ammonium head neutralizes acidic groups on graphene oxide, like carboxyl or hydroxyl groups, reducing free hydrogen ions (H+) concentration and increasing hydroxide ions (OH−).

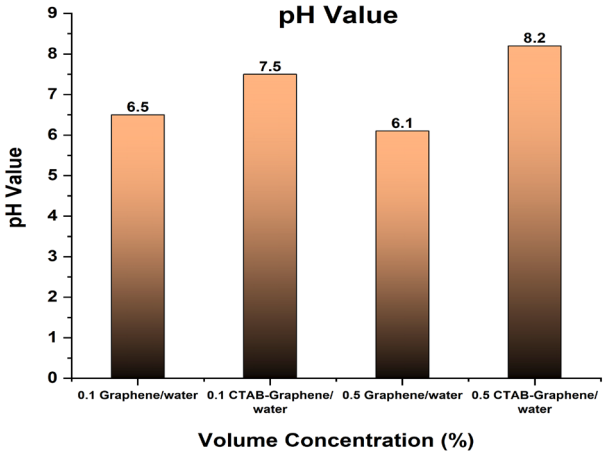

Fig. 10. pH Value for GPN/ water nanofluids.

Additionally, CTAB can aid graphene reduction, consuming H+ ions. At higher concentrations, CTAB micelle formation further contributes to the solution's alkalinity with 0.1 vol % concentration, the pH remains close to 7.5 but increases to 0.5% (8.2), as shown in Fig. 10.

4.3. Comparison of Al_2O_3 Vs graphene

Al_2O_3 nanofluids demonstrate greater acidity compared to graphene-based ones. When alumina nanoparticles are dispersed in water, they undergo slight hydrolysis, releasing acidic components and resulting in pH values ranging from 5 to 7, contingent on concentration and additives. In contrast, graphene nanofluids maintain a pH between 6 and 8, which is neutral to slightly alkaline, particularly when minimally functionalized. Consequently, alumina-based nanofluids are more acidic than their graphene counterparts [44].

Particle size trends vary with concentration changes in different ways for each nanofluid type. In graphene/water nanofluids, higher concentrations lead to smaller particle sizes due to graphene's structure and the CTAB surfactant. Conversely, in alumina/water nanofluids, increased concentration results in larger particle sizes because of weaker van der Waals forces. CTAB enhances dispersion in both types, but its effect is more pronounced in graphene nanofluids due to graphene's planar geometry and surface area.

When alumina (Al_2O_3) replaced graphene in water nanofluids with CTAB added, particle size increased. Alumina nanoparticles, typically ranging from 30 to 100 nm, are larger than graphene due to their morphology. Although CTAB reduces aggregation and improves dispersion, alumina particles remain larger, and CTAB's size reduction effect is less significant with alumina. Alumina nanoparticles have a higher tendency to aggregate than graphene, reducing dispersion stability in water. Even though CTAB helps reduce aggregation, alumina tends to form larger aggregates, which leads to lower thermal conductivity and higher viscosity when compared to graphene-based nanofluids. However, alumina nanofluids can still improve thermal properties and are appropriate for applications that need stable, non-corrosive materials, although their performance is not as good as that of graphene-based nanofluids.

Without CTAB, graphene nanofluids showed low zeta potential and poor dispersion stability. When CTAB was added, it increased the zeta potential by giving a positive charge to the graphene surface, which enhanced electrostatic repulsion and improved both stability and dispersion. In a similar manner, alumina nanofluids without CTAB also had low zeta potential and stability issues. The introduction of CTAB improved the zeta potential by positively charging the alumina particles, which enhanced their dispersion. However, this improvement was not as pronounced as in graphene nanofluids, due to the larger particle size and different surface chemistry of alumina, leading to somewhat reduced stability.

5. Results and discussion

5.1. Thermal conductivity analysis

The current study results reveal that adding Alumina and GPN to water suspensions, combined with CTAB surfactant, substantially enhances thermal conductivity. The choice of surfactant notably amplified thermal conductivity of nanofluids due to its effect on ballistic phonon movement. Thermal conductivity measurements in nanofluids containing Alumina, GPN, and CTAB at various concentrations showed consistent trends across all samples. Fig. 11 illustrates the thermal conductivity enhancement in relation to temperature and volume concentration. The thermal conductivity of alumina/water increased markedly with temperature and concentration. At 30℃, a 0.1 vol. % concentration yielded a 4.28% increase, while a 0.5 vol. % concentration produced a 7.65% rise. Nanofluids with Alumina and CTAB in a 1:0.5 ratio showed even greater improvements, with 6.65% and 9.95% increases at 0.1 and 0.5 vol. % concentrations respectively, at the same temperature. When the temperature was raised to 70 °C, the alumina/water nanofluids exhibited more significant increases: 10.1% at 0.1 vol. % and 19.81% at 0.5 vol. %. CTAB Alumina/water nanofluids at 70℃ demonstrated the most substantial enhancements, reaching 13.85% and 23.67% for the same concentrations. Regarding the temperature effect on the alumina/water nanofluid at 0.1 vol. %, the increase ranged from 4.28 to 10.16 for 30℃ and 70℃ respectively, compared to water. Likewise, the CTAB-Alumina/water nanofluid at 0.1% showed an increase from 6.65 to 13.85 for 30℃ and 70 °C. Lastly, the 0.5% CTAB-alumina/water nanofluid increased from 9.59% at 30 °C to 23.67% at 70 °C. This thermal conductivity enhancement is attributed to temperature and surfactant addition, which contribute to stability. Multiple studies have shown that increasing temperature leads to improved thermal conductivity in nanofluids [45,46].

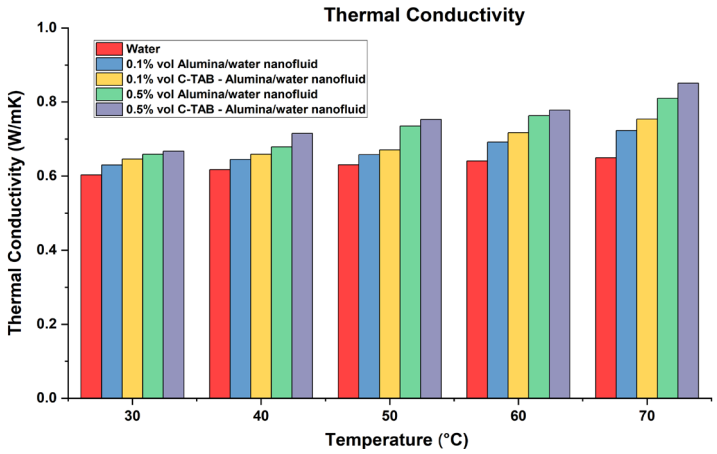

Fig. 11. Thermal conductivity of alumina/ water nanofluids combination.

Similarly, with Graphene/water concentration of 0.1 vol. %, thermal conductivity enhancement reached 6.30%, while at 0.5 vol. %, it increases to 13.76%, both at 30 ℃as shown in the Fig 12. Nanofluids with a 1:0.5 ratio of Graphene/CTAB at 0.1 and 0.5 vol. % showed notable thermal conductivity improvements of 8.29% and 14.26% respectively at 30 ℃. In contrast, the graphene/water nanofluid at 0.1 and 0.5 vol. % displayed thermal conductivity enhancements of 24.09% and 32.56% at 70℃, respectively. At 70℃, the CTAB Graphene/water nanofluid exhibited increases of 27.48% and 33.79%, respectively. For GPN/water nanofluid at 0.1 vol. %, the temperature effect resulted in an increase from 6.30 to 24.09 between 30℃ and 70 ℃. Likewise, CTAB-GPN/water nanofluid at 0.1% showed an increase from 8.29 to 27.48 between 30℃ and 70 ℃. The 0.5% CTAB-GPN/water nanofluid increased from 14.2% at 30 °C to 33.79% at 70 °C. This occurs as higher temperatures induce greater kinetic energy, enhancing thermal conductivity in

the stable nanofluid due to the zeta potential. GPN-based nanofluids surpass alumina nanoparticles in performance because of their shape, size, and thermal conductivity.

The enhanced dispersion and stability of nanoparticles resulted in an advantageous increase in heat conductivity. Additional reported mechanism comprises Brownian motion, liquid stratification, and nanolayer aggregation. Consequently, it may be inferred that the incorporation of nanoparticles into fluids via a surfactant, as demonstrated in this study, is essential for enhancing thermal conductivity. Surfactant application must be meticulously regulated to avoid affecting viscosity measurements.

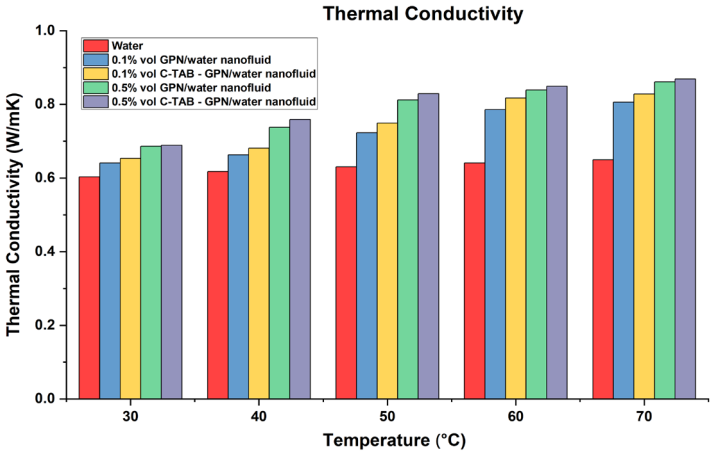

Fig. 12 Thermal conductivity of GPN/ water nanofluids combination.

5.2. Viscosity

The correlation between viscosity and temperature for Alumina/water and Graphene/water nanofluids at 0.1 and 0.5 vol. % concentrations, with and without CTAB surfactant in a 1:0.5 ratio, is illustrated in Fig. 13. The findings revealed that all nanofluid varieties, regardless of nanoparticle composition, demonstrated higher viscosity at increased concentrations when compared to pure water. Significantly, the incorporation of CTAB into both alumina/water and graphene/water nanofluids led to the highest observed viscosity measurements. Conversely, nanofluid samples lacking CTAB exhibited the lowest viscosity values among all tested specimens.

The alumina/water nanofluids demonstrated varying viscosity increases based on concentration and temperature. At 30 ℃, a 0.1 vol. % concentration showed a 33.70% increase, while a 0.5 vol. % concentration exhibited a 49.68% rise. Nanofluids containing Alumina and CTAB in a 1:0.5 ratio displayed even higher increases, with 49.05% and 58.95% rises at 0.1 and 0.5 vol. % concentrations, respectively, at the same temperature. When the temperature was raised to 70 °C, the alumina/water nanofluids showed more significant increases: 110.64% at 0.1 vol. % and 111.3% at 0.5 vol. %. CTAB Alumina/water nanofluids at 70 ℃ exhibited the most substantial increases, reaching 113.64% and 127.47% for the same concentrations.

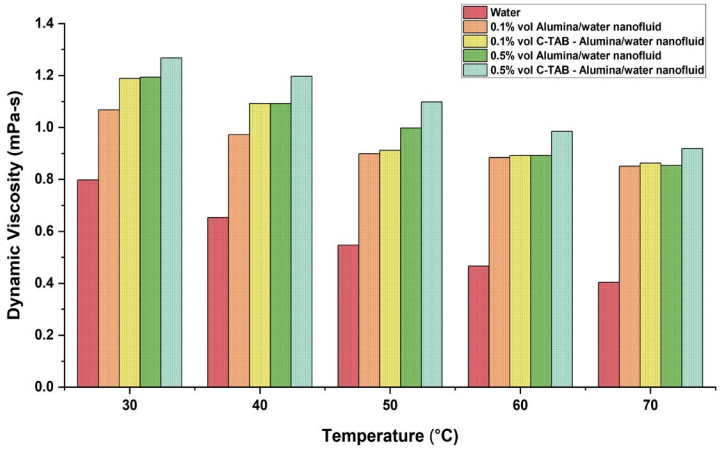

Fig. 13. Dynamic viscosity of alumina/ water nanofluids combination

Analysis of the result indicated that at lower alumina concentrations (0.1 vol. %), the viscosity increase was relatively modest compared to water. The addition of CTAB surfactant resulted in more pronounced increases: 33.76% and 49.05% at 30 °C and 110.64% and 113.61% at 70 °C, respectively, when compared to water. Higher Alumina concentrations (0.5 vol. %) led to more significant viscosity increases: 49.68% without surfactant and 58.95% with CTAB at 30 °C. These increases were further amplified at 70 °C, reaching 111.38% and 127.47%, respectively.

The dynamic viscosity of graphene/water nanofluid increased by 44.09% at 0.1 vol. % and 70.42% at 0.5 vol. %, both at 30°C as shown in Fig 14. Nanofluids containing a 1:0.5 ratio of Graphene/CTAB exhibited even greater viscosity increases of 57.70% and 82.02% at 0.1 and 0.5 vol. %, respectively, at the same temperature. At 70°C, the graphene/water nanofluid showed viscosity increases of 118.63% and 144.79% for 0.1 and 0.5 vol. % concentrations, while the CTAB Graphene/water nanofluid demonstrated increases of 121.28% and 165.84%, respectively. Examination of the data indicated that at lower graphene concentrations (0.1 vol. %), the viscosity increase was minimal compared to water. The introduction of CTAB resulted in more pronounced increases: 44.09% and 57.70% at 30 °C, and 118.63% and 121.28% at 70 °C, respectively, when compared to water. At higher graphene concentrations (0.5 vol. %), the viscosity increase was more significant: 70.42% without surfactant and 82.02% with CTAB at 30 °C. These increases were even more substantial at 70 °C, reaching 144.79% and 165.82%, respectively.

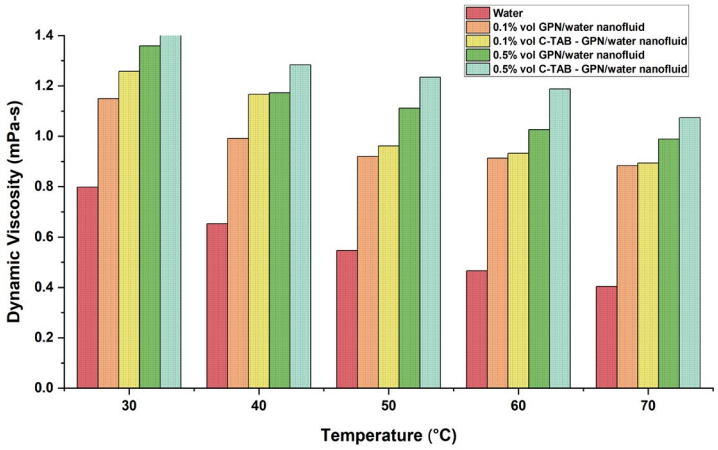

Fig. 14. Dynamic viscosity of GPN / water nanofluids combination.

The specific type of CTAB surfactant played a significant role in determining nanofluid viscosity. Results indicate that combinations of CTAB with graphene and alumina produce substantially higher viscosities than those without CTAB. Although CTAB addition improves zeta potential values in nanofluids, it becomes evident that viscosity is primarily controlled by two key factors: volume concentration and temperature [47]. The addition of nanoparticles like Graphene, Alumina, and Surfactant to the base fluid considerably increased the shear force. Simultaneously, rising temperatures weaken intermolecular bonds, resulting in increased kinetic energy and subsequent viscosity decrease [48]. These results align with the findings of the current study.

6. Conclusion

An extensive investigation examined the preparation and stability of alumina and GPN nanofluids, with a focus on their thermal conductivity and viscosity properties. The study utilized a two-step method to create nanofluids at 0.1 and 0.5 volume concentrations. Thermal conductivity and viscosity measurements were conducted on these samples across a temperature range of 30–70 °C. This comprehensive research yielded a set of significant outcomes.

Analyses of the zeta potentials of alumina/water CTAB nanofluids revealed an increase of up to +37 mV at 0.1 vol %, while graphene/water CTAB nanofluids showed an increase of up to +35 mV at 0.5 vol %.

The particle size distribution of the alumina nanofluid was quite narrow, with the majority of particles measuring between 50-100 nm in diameter. On the other hand, the GPN nanofluid displayed a wider size distribution, with particles ranging from 20-200 nm. Over a 30-day assessment, the stability of both colloidal solutions was evaluated, showing that the alumina nanofluid retained its dispersion more effectively than the GPN nanofluid, which began to show signs of agglomeration and sedimentation after just two weeks.

The thermal conductivity of the nanofluid being studied increased with higher solid concentrations. Additionally, it exhibited an upward trend as the temperature rose.

Maximum increases in thermal conductivity were 27.48% and 33.79% for the CTAB GPN/water nanofluid and 10.6% and 19.81% for the CTAB alumina/water nanofluid at concentrations of 0.1 and 0.5 vol%, respectively.

Viscosity of nanofluids increased with concentration and decreased with temperature rise. The CTAB GPN/water nanofluid had a maximum viscosity increase of 121.28% and 165.84% at 70 °C, whereas the CTAB Alumina/water nanofluids showed increases of 110.64% and 111.3%.

The findings underscore the importance of regulating nanoparticle dispersion to enhance nanofluid stability. The addition of nanoparticles proves beneficial for improving the thermal conductivity of nanofluids, thereby enhancing heat transfer efficiency. This phenomenon indicates the existence of an optimal albumin and GPN concentration at which the nanofluid's particle dimensions and viscosity result in notable thermal conductivity improvements. Interestingly, increasing the concentration beyond this optimal point yields no substantial additional benefits in terms of thermal conductivity enhancement.

Acknowledgement

The author gratefully acknowledges Dr. Suresh S, Professor and Head of the Department of Mechanical Engineering, NIT Trichy, and Dr. Saravanan Dhandayutham, Associate Professor, National College Instrumentation Facility (NCIF), Trichy, for their valuable support in analytical insights and technical discussions that significantly contributed to this work.

References

[1] D. Dewanjee , B. Kundu, Renewable Energy 240, 122182 (2025); https://doi.org/10.1016/j.renene.2024.122182.
[2] S.Asadi, A. Aberoumand, F. Moradikazerouni, et al. Powder Technology 352, 209–226.2019; https://doi.org/10.1016/j.powtec.2019.04.054.
[3] B.Mehta, D. Subhedar, H. Panchal, et al. International Journal of Thermofluids 20, 100410 (2023); https://doi.org/10.1016/j.ijft.2023.100410.
[4] G. Marseglia, M. Sanches, A.P.Ribeiro, et al. Applied Thermal Engineering 210, 118411 (2022); https://doi.org/10.1016/j.applthermaleng.2022.118411
[5] U.S. Behera, J.S. Sangwai, H.S.Byun, Renewable and Sustainable Energy Reviews 207, 114901 (2025); https://doi.org/10.1016/j.rser.2024.114901
[6] D. Akhgar, Toghraie, Powder Technology 338 806–818 (2018); https://doi.org/10.1016/j.powtec.2018.07.086.
[7] M.I.Shajahan, J.J. Michael, M. Arulprakasajothi, et al. Energies, 13, 4554 (2020); https://doi.org/10.3390/en13174554.
[8] S. Mohamed Iqbal, S. Christopher, M. Jee Joe et al. International Journal of Thermal Sciences 183, 107844 (2023); https://doi.org/10.1016/j.ijthermalsci.2022.107844.
[9] A. Hutin, M.S. Carvalho, Powder Technology 399, 117157 (2022); https://doi.org/10.1016/j.powtec.2022.117157.
[10] A.H. Pordanjani, S.Aghakhani, M. Afrand , et al. Energy Conversion and Management 198, 111886 (2019); https://doi.org/10.1016/j.enconman.2019.111886.
[11] A.O Borode, A. Noor, A.Ahmed, P. A. Olubambi, Nano-Structures & Nano-Objects 20, 100394 (2019); https://doi.org/10.1016/j.nanoso.2019.100394
[12] J. M. Salehi, A. Rajabpour, M.M.Heyhat, Applied Physics Letters, 102(23), 231907 (2013); https://doi.org/10.1063/1.4809998.
[13] S.M. Iqbal, C.S. Raj, J.J. Michael, A.M. Irfan, Digest Journal of Nanomaterials & Biostructures, 12(2), 255–263 (2017);
[14] I.H, Ghadimi, Metselaar, Experimental Thermal Fluid Science 51, 1–9 (2013); https://doi.org/10.1016/j.expthermflusci.2013.06.001
[15] K. Cacua, F. Ordoñez, C. Zapata, B. Herrera, et al. Colloids and Surfaces A: Physicochemical and Engineering Aspects 583, 123960 (2019); https://doi.org/10.1016/j.colsurfa.2019.123960.
[16] D. Zhu, X. Li, N. Wang, X. Wang, J. Gao, H. Li, Current Applied Physics 9 131–139, (2009); https://doi.org/10.1016/j.cap.2007.12.008.
[17] M. Mehrali, E. Sadeghinezhad, S.T. Latibari et al. Nanoscale Research Letters 9, 15 (2014);
[18] F.R. Siddiqui, C.Y. Tso, K.C. Chan, S.C. Fu, C.Y.H. Chao, International Journal of Heat and Mass Transfer 132, 1200 -1216 (2019); https://doi.org/10.1016/j.ijheatmasstransfer.2018.12.094.
[19] Z. Said, Process Safety and Environmental Protection 188, 1221-1234 (2024); https://doi.org/10.1016/j.psep.2024.05.141.
[20] K.R. Priya, K.S. Suganthi, K.S. Rajan, International Journal of Heat and Mass Transfer 55 (17–18), 4734–4743 (2012); https://doi.org/10.1016/j.ijheatmasstransfer.2012.04.035
[21] H. Huang, C. Li, S. Huang, Y. Shang, Journal of Molecular Liquids, 393,123652 (2024); https://doi.org/10.1016/j.molliq.2023.123652.
[22] M.F. Zawrah, R.M. Khattab, L.G. Girgis, et al. HBRC Journal 12, 1–8 (2016); https://doi.org/10.1016/j.hbrcj.2014.12.001.
[23] H.R.Kulkarni, C. Dhanasekaran, P. Rathnakumar, S. Mohamed Iqbal, S. Sivaganesan, Materials Today: Proceedings, 58(1), 104-113 (2022); https://doi.org/10.1016/j.matpr.2022.01.079.
[24] S. Hamze, D. Cabaleiro, P. Estellé, Journal of Molecular Liquids 325 115207 (2021); https://doi.org/10.1016/j.molliq.2020.115207.
[25] Esfahani, M. Rabbani, E.M. Languri, International Communications in Heat and Mass Transfer 76 308-315 (2016); https://doi.org/10.1016/j.icheatmasstransfer.2016.06.006.
[26] P. Yuri, F. Shabiev, R. Safargaliev et al. Journal of Molecular Liquids 361, 119551 (2022); https://doi.org/10.1016/j.molliq.2022.119551.

[27] M. Mehrali, E. Sadeghinezhad, S. Tahan Latibari, Journal of Materials Science 49, 7156–7171 (2014); https://doi.org/10.1007/s10853-014-8424-8.
[28] B. Nazari, Z. Ranjbar, R.R. Hashjin, A. Rezvani Moghaddam, G. Momen, B. Ranjbar, Colloids Surface A: Physicochemical Engineering Aspects 582, 123870 (2019); https://doi.org/10.1016/j.colsurfa.2019.123870.
[29] S.U. Ilyas, S. Ridha, F.A. Abdul Kareem, Colloids Surface A: Physicochemical Engineering Aspects 592 124584, (2020); https://doi.org/10.1016/j.colsurfa.2020.124584
[30] M.A. Morozova, A.A. Osipov, E.A. Maksimovskiy, A.V. Zaikovsky, Nano-Structures & Nano-Objects 40, 101409 (2024); https://doi.org/10.1016/j.nanoso.2024.101409.
[31] C. Selvam, T. Balaji, D. Mohan Lal, S. Harish, Experimental Thermal Fluid Science 80, 67–76 (2017); https://doi.org/10.1016/j.expthermflusci.2016.08.013.
[32] P. Sundaram, A. Kalaisselvan, A. Sathishkumar, Journal of Energy Storage 64,107219 (2023); https://doi.org/10.1016/j.est.2023.107219.
[33] M. Fares, M. AL-Mayyahi, M. et al. Case Studies in Thermal Engineering 18, 100584. (2020); https://doi.org/10.1016/j.csite.2020.100584.
[34] A. Amiri, R. Sadri, M. Shanbedi, G. Ahmadi, BT. Chew, SN. Kazi SN, et al. Energy Conversation Management 92, 322–30 (2015); https://doi.org/10.1016/j.enconman.2014.12.051.
[35] S. Askari, A. Rashidi, H. Koolivand, International Communication in Heat Mass Transfer 108 104334 (2019); https://doi.org/10.1016/j.icheatmasstransfer.2019.104334.
[36] A. Ngqalakwezi, D. Nkazi, G. Seifert, T. Ntho, Catalysis Today, 358, 338–344 92019); https://doi.org/10.1016/j.cattod.2019.06.029.
[37] J. Li, Q.Liu, R.A. Flores, J. Lemmon, T. Bligaard, Physical Chemistry Chemical Physics, 22(10), 5969–5975 (2020); https://doi.org/10.1039/c9cp06394c.
[38] M. Tawalbeh, I. Shomope, A. et al. International Journal of Thermofluids, 22, 100705 (2024); https://doi.org/10.1016/j.ijft.2024.100705
[39] J. Du, Y. Wang, W. Yang, J. Wang, Z. Cao, B, Sundén, International Journal of Heat and Mass Transfer, 221, 125080 (2023); https://doi.org/10.1016/j.ijheatmasstransfer.2023.125080.
[40] P. Kanti, C. G. Ramachandra, B. Panitapu, K.V. Sharma, Heat Transfer, 49(8), 4722–4737 (2020); https://doi.org/10.1002/htj.21849.
[41] T. Ambreen, M.H. Kim, International Journal of Heat and Mass Transfer, 120, 490–498 (2017); https://doi.org/10.1016/j.ijheatmasstransfer.2017.12.067.
[42] R. Marsalek, R. Jarusek, E. Volna, M. Kotyrba, Mathematics, 9(23), 3089 (2013); https://doi.org/10.3390/math9233089.
[43] M. A Rahman, S.M.M. Hasnain, S. Pandey, Tapalova, et al. ACS Omega, 9(30) (2024); https://doi.org/10.1021/acsomega.4c03279.
[44] M. Zareei, H. Yoozbashizadeh, et al. Journal of Thermal Analysis and Calorimetry, 135(2), 1185–1196 (2018); https://doi.org/10.1007/s10973-018-7620-1.
[45] A. Rehman, S. Yaqub, S., M.Ali, H. Nazir, et al. Journal of Molecular Liquids, 391, 123350; https://doi.org/10.1016/j.molliq.2023.123350.
[46] P. K. Das, N. Islam, A.K. Santra, R. et al. Journal of Molecular Liquids, 237, 304–312 (2017); https://doi.org/10.1016/j.molliq.2017.04.099
[47] Kaggwa, A., Walmsley, M., Carson, J. K., & Atkins, M. (2019). Materials Today: Proceedings, 18, 510–519. https://doi.org/10.1016/j.matpr.2019.06.240.
[48] M.I. Shajahan, C. Sundar Raj, S. Arul, P. Rathnakumar. *Journal of Advances in Chemistry*, **13**(3), 1–8 (2017); https://rajpub.com/index.php/jac/article/view/4530.